Journal of Controlled Release 236 (2016) 79–89

Contents lists available at ScienceDirect

Journal of Controlled Release

journal homepage: www.elsevier.com/locate/jconrel

A site-selective hyaluronan-interferonα2a conjugate for the treatment of ovarian cancer

Isabella Monia Montagner [a], Anna Merlo [a], Debora Carpanese [b], Anna Dalla Pietà [b], Anna Mero [c], Antonella Grigoletto [c], Arianna Loregian [d], Davide Renier [e], Monica Campisi [e], Paola Zanovello [a,b], Gianfranco Pasut [a,c,*,1], Antonio Rosato [a,b,**,1]

[a] Veneto Institute of Oncology IOV-IRCCS, Padua, Italy
[b] Department of Surgery, Oncology and Gastroenterology, University of Padua, Padua, Italy
[c] Department of Pharmaceutical and Pharmacological Sciences, University of Padua, Padua, Italy
[d] Department of Molecular Medicine, University of Padua, Padua, Italy
[e] Fidia Farmaceutici SpA, Abano Terme, Italy

ARTICLE INFO

Article history:
Received 9 December 2015
Received in revised form 23 June 2016
Accepted 24 June 2016
Available online 26 June 2016

Keywords:
Ovarian cancer
Tumor targeting
Interferon
HAylation
Hyaluronan

ABSTRACT

While interferon alpha (IFNα) is used in several viral and cancer contexts, its efficacy against ovarian cancer (OC) is far from being incontrovertibly demonstrated and, more importantly, is hindered by heavy systemic side effects. To overcome these issues, here we propose a strategy that allows a targeted delivery of the cytokine, by conjugating IFNα2a with an aldehyde-modified form of hyaluronic acid (HA). The resulting HA-IFNα2a bioconjugate was biochemically and biologically characterized. The conjugation with HA did not substantially modified both the antiviral function and the anti-proliferative activity of the cytokine. Moreover, the induction of STAT1 phosphorylation and of a specific gene expression signature in different targets was retained. *In vivo* optical imaging biodistribution showed that the i.p.-injected HA-IFNα2a persisted into the peritoneal cavity longer than IFNα2a without being toxic for intraperitoneal organs, thus potentially enhancing the loco-regional therapeutic effect. Indeed, in OC xenograft mouse models bioconjugate significantly improved survival as compared to the free cytokine. Overall, HA-IFNα2a bioconjugate disclosed an improved anticancer efficacy, and can be envisaged as a promising loco-regional treatment for OC.

1. Introduction

Interferon (IFN) is a family of related cytokines composed of two classes, Type-I and Type-II, which regulate various cellular functions. Type-I IFN consists of seven components, with the predominant forms being IFNα that in humans comprises 12 separate proteins, and one IFNβ [1,2]. The main IFN signaling pathway is very rapid and, after the extracellular binding of the cytokine, results in the activation of intracellular Janus kinase that phosphorylates a specific tyrosine residue in the STAT protein, thus inducing the transcription of IFN-inducible genes [3,4]. Different Type-I IFNs exhibit a wide range of biological effects, because they mediate anti-viral activities, and potentiate antitumor immune responses [5–8].

All these features make IFNs effective antitumor and antiviral molecules to treat different pathologies [9,10]. Indeed, IFNα is widely used in the treatment of viral diseases (hepatitis B and C) [11], and is employed in clinical oncology against a broad spectrum of cancers including some hematological malignancies (hairy cell leukemia, chronic myeloid leukemia, some B- and T-cell lymphomas) [12], and solid tumors (melanoma, renal carcinoma and Kaposi's sarcoma) [13–15]. In particular, IFNα was the first cytokine that received FDA approval for the treatment of leukemia and melanoma [16].

The efficacy of IFN in the treatment of ovarian cancer (OC) is still under investigation, with encouraging results registered in a phase I/II study [17]. Notwithstanding, the debilitating side-effects of this agent remain a great challenge for the use of this noteworthy therapeutic potential [18]. On the other hand, the use of type-I IFN has been poorly effective, largely due to toxic effects. To overcome the systemic side-effects, several IFN delivery systems have been developed, such as the conjugation with polyethylene glycol (PEG) [13,19], gene delivery by albumin fusion protein [20], and microspheres for a constant release [21,22].

Based on our previous studies with HA-protein and HA-drug conjugates [23–27], we hypothesized that HAylation of IFNα2a, namely the

* Correspondence to: G. Pasut, Department of Pharmaceutical and Pharmacological Sciences, University of Padua, Padua, Via F. Marzolo 5, I-35131 Padova, Italy.
** Correspondence to: A. Rosato, Department of Surgery, Oncology and Gastroenterology, University of Padua, Via Gattamelata 64, I-35128 Padova, Italy.
E-mail addresses: gianfranco.pasut@unipd.it (G. Pasut), antonio.rosato@unipd.it (A. Rosato).
[1] Senior co-authorship.

http://dx.doi.org/10.1016/j.jconrel.2016.06.033

covalent link of HA, could represent a good strategy for the intraperitoneal local targeted delivery of the cytokine in ovarian cancer patients. HA was chosen because this polysaccharide is naturally present in several body compartments, and hence fully biocompatible [28]. Moreover, all the biological processes in which HA is involved (morphogenesis, wound repair, inflammation and cancer metastasis) [29] are mediated by HA receptors, in particular CD44 that is overexpressed in many cancer types including the ovarian histotype [30]. Therefore, as the CD44 receptor confers specificity and selectivity for cancerous cells being a target site for HA-based drug delivery systems [31], the conjugation of IFNα2a to HA is expected to decrease the toxicity induced in patients by free IFNα2a.

In this work, we report the synthesis and chemical/biological characterization of a novel HA-IFNα2a bioconjugate, demonstrating that it retains a good level of antiviral and anti-proliferative activities with respect to the original free cytokine, but is endowed with higher therapeutic efficacy when administered locally in an OC intraperitoneal xenograft model. Therefore, HA-conjugation improves the anticancer efficacy of IFNα2a and supports further testing as a promising loco-regional approach for the treatment of ovarian cancer.

2. Materials and methods

2.1. Chemicals and drugs

Interferon-α2a (IFNα2a) was supplied by GenScript (Piscataway, USA), while hyaluronic acid sodium salt (HA, MW 200 kDa) was from Fidia Farmaceutici S.p.A. (Abano Terme, Italy). CH_3SO_3H, 1,1′-carbonyldiimidazole (CDI), triethylamine (Et_3N), 4-aminobutyraldehyde diethyl acetal, D_2O and all the other chemical reagents, including salts and solvents, were purchased from Sigma-Aldrich (Milan, Italy).

2.2. Synthesis of HA-acetal

HA sodium salt (100 mg, 0.25 mmol) was dissolved in 10 mL of DMSO (dimethyl sulfoxide) with CH_3SO_3H (81 μL, 1.25 mmol). After complete dissolution, about 1–2 h, CDI (203 mg, 1.25 mmol) was added, followed after 1 h by the addition of 4-aminobutyraldehyde diethyl acetal (0.25 mmol). Et_3N was used, if necessary, to raise the pH to 8.0. The reaction mixture was left to stir at 40 °C for 12 h, and then 1 mL of NaCl saturated solution was added drop wise, till the organic solution became opalescent. After 30 min of mixing, the polymer was precipitated slowly by adding 20 mL of chilly ethanol. The precipitate was washed with EtOH/H_2O solutions at increasing percentage of ethanol (70:30, 80:20, 90:10, v/v), and filtered after each step. To better purify the product from unreacted amine, the dried polymer was dissolved in water and extensively dialyzed against demineralized water before lyophilization. The derivatization degree was determined by ^1H NMR by comparing the integration values of methylene H of acetal moiety with the acetyl H of HA backbone.

^1H NMR HA-acetal (300 MHz, D_2O, 25 °C, δ): 1.10 (t, 6H, integration value reflected the degree of activation, –CH(OCH_2-CH_3)$_2$, acetal moiety), 1.85 (s, 3H, —NHCO-CH_3, HA), 3.2–3.8 (m, GlcA, GlcNAc methylene H, methane-H, HA).

2.3. Synthesis of N-terminal HA-IFNα2a conjugate

HA-acetal (4 mg; degree of acetal modification 4% mol) was dissolved in 600 μL of 25 mM H_3PO_4 pH 2.1 and stirred for 1 h at 60 °C. After cooling to room temperature (RT), the pH value of the solution was raised to 6.0 with 0.1 M NaOH. IFNα2a (1.6 mg), previously dissolved in 2.4 mL of 0.1 M Na_2HPO_4 buffer pH 6.0, was added. After 1 h, $NaBH_3CN$ (3 mg, 21.9 μmol), dissolved in 20 μL of 0.1 M Na_2HPO_4 buffer pH 6.0, was added and the reaction was stirred at RT for 48 h. Then, 5 equivalent of glycine, with respect to each equivalent of aldehyde in the starting HA, were added to the reaction mixture to quench all the aldehyde groups. The reaction was analyzed by SEC (size-exclusion chromatography) with an analytical Zorbax GF-250 column (250 × 4.6 mm), eluted with 20 mM Na_2HPO_4, 130 mM NaCl pH 7.0, at a flow rate of 0.3 mL/min. The UV–vis detector was settled at 226 nm. The purification was carried out with a semi-preparative GF-250 (250 × 9.4 mm) eluted with the same buffer used above at the flow rate of 1 mL/min. The purified conjugate was concentrated to 10 mL and the purity was confirmed by analytical SEC. The product was extensively dialyzed against demineralized water and lyophilized. The total protein content was determined by the average of the results obtained by bicinchoninic acid colorimetric assay and Abs 0.1% at 280 nm.

2.4. Characterization of HA-IFNα2a

2.4.1. Near-UV circular dichroism

Near-UV CD spectra were measured using a Jasco J-810 spectropolarimeter equipped with a Peltier temperature control unit settled at 20 °C. Measurements of IFNα2a and HA-IFNα2a were performed in PBS (phosphate buffered saline), pH 7.2. The concentration of protein in all the samples was of 1 mg/mL as determined spectrophotometrically at 280 nm. The contribution of HA was negligible, as it did not have any absorbance at that wavelength. The spectra were collected over the wavelength range of 250–320 nm with an average of 2 scans. The sample cell path length was 1 mm. The CD data were converted to mean residue ellipticity, expressed in deg. cm^2 $dmol^{-1}$ by applying the following formula:

$$\Theta = \Theta obs\,(MRW)/10\ L\,[C]$$

where Θ is the observed ellipticity in degrees, MRW is the mean residue weight of the peptide (molecular weight divided by the number of residues), [C] is the peptide concentration in mg/mL, and L is the optical path length in centimeters.

2.4.2. Determination of the site of HA conjugation

Native and HAylated IFNα2a (0.1 mg protein equiv.) were dissolved in 6 M guanidinium·HCl, 50 mM Tris-HCl (pH 9.0) to reach a protein concentration of 1.0 mg/mL. In order to reduce disulphide bridges, tris(2-carboxyethyl)phosphine hydrochloride was added to the protein solution at the final concentration of 5 mM and the reaction mixture was kept for 1 h at 37 °C. To the reduced protein, iodoacetamide was added to the final concentration of 25 mM. S-alkylation was allowed to proceed for 30 min at 37 °C in the dark. Protein samples were purified by RP-HPLC on a Phenomenex Jupiter C18 column (250 × 4.6 mm; 5 μm) at a flow-rate of 1.0 mL/min, detection at 226 nm, eluted with a solvent gradient of water/ACN both containing 0.1% (v/v) TFA. Gradient 0′–5% ACN, 5′–40% ACN, 25′–80% ACN, 27′–90% ACN, 30′–5% ACN. The collected peaks were lyophilized. The reduced and S-carboxamidomethylated samples of IFNα2a and HA-IFNα2a were dissolved in 8 M urea and diluted in 50 mM phosphate buffer (pH 7.9) to reach a final IFNα2a concentration of 1 mg/mL and urea concentration of 0.8 M. An aliquot of trypsin of peptide sequencing purity grade was then added at an E/S ratio of 1:50 (w/w), and the proteolysis was allowed to proceed at 37 °C overnight. The digestion mixtures, desalted by PepClean C-18 Spin columns (Pierce, Rockford, IL), were analyzed by an UPLC-Q-TOF mass spectrometry method with a Grace Vydac TP C18 column (150 × 1 mm; 5 μm), maintained at 32 °C, flow-rate 0.05 mL/min, detection at 280 nm, eluted with a solvent gradient of water/ACN both containing 0.1% formic acid. Gradient 3′–3% ACN, 24′–80% ACN, 28′–80% ACN, 29′–3% ACN, 35′–3%. Mass spectrometry data of the tryptic fragments and the chromatographic peaks of native and HAylated IFNα2a were compared to identify the site of HA conjugation.

2.5. Tumor cell lines

The following human cancer cell lines were used: HCT-15, HT-29, LoVo and Caco-2, colorectal adenocarcinoma (CRC); IGROV-1, OVCAR-3 and SKOV-3, ovarian adenocarcinoma; PD-OVCA1 is a primary human ovarian cancer cell line isolated and propagated in our institution [32]. $CD44^{high}$ and $CD44^{low}$ subpopulations of HCT-15 were previously isolated by immunomagnetic sorting [26]. Cells were cultured in RPMI 1640 (EuroClone, Milan, Italy) supplemented with 10% (v/v) heat-inactivated fetal bovine serum (Gibco BRL, Paisley, UK), 2 mM L-glutamine (Lonza, Verviers, Belgium), 10 mM HEPES (Lonza), 100 U/mL penicillin/streptomycin (Lonza), hereafter referred as to complete medium. The African green monkey kidney-derived VERO cell line was grown in Eagle's minimum essential medium (Sigma-Aldrich) with supplements as describe above. Cell lines were maintained at 37 °C in a humidified atmosphere containing 5% CO_2.

2.6. Antiviral assay

To determine IFNα2a-induced antiviral effects, VERO cell line was resuspended in complete medium and seeded into 96-well flat-bottomed plates (1×10^5/well) with different concentrations of IFNα2a, HA-IFNα2a and HA 200 kDa (negative control) for 24 h. At day 1, cells were infected with vesicular stomatitis virus (VSV; MOI 1) and the day after the viability was assessed by the ATPlite luminescence adenosine triphosphate detection assay system (PerkinElmer, Zaventem, Belgium), according to the manufacturer's instructions. The lysis solution was added to each well (50 μL), followed by addition of 50 μL of substrate solution and finally the luminescence was counted by the TopCount Microplate Counter (PerkinElmer). Within each experiment, determinations were performed in triplicate and experiments were repeated four times. The percentage of cell survival was calculated by determining the counts per second (cps) values according to the formula: $[(cps_{tested} - cps_{blank}) / (cps_{untreated\ control} - cps_{blank})] \times 100$, with cps_{blank} referring to the cps of wells that contained only medium and ATPlite solution. The IC_{50} values were calculated from semi-logarithmic dose-response curves by linear interpolation. Moreover, to visualize the interferon activity, cells treated as described above were fixed with a mixture of methanol and acetic acid (2:1) for 30 min at 4 °C. Subsequently, the medium from each well was aspirated, washed twice with milliQ water and stained over-night with crystal violet 2% (w/v) at 4 °C. After the crystal violet solution was decanted, the plate was rinsed with milliQ water and then dried in air.

2.7. Antiproliferative assay

To assess the IFNα2a antiproliferative activity, human colorectal and ovarian cancer cell lines were resuspended in complete medium and seeded into 96-well flat-bottomed plates (8×10^4/well). The day after, different concentrations of IFNα2a, HA-IFNα2a and HA 200 kDa were added (final volume, 100 μL/well) for 72 h. Finally, the cytotoxicity assay was performed at day 4 by the ATPlite assay system, as reported above. Within each experiment, determinations were performed in triplicate and experiments were repeated 5 times for each cell line.

2.8. Flow cytometry analysis

CD44 expression in all tumor cell lines was evaluated by flow cytometry, as previously reported [27]. Peripheral blood mononuclear cells (PBMC) were isolated from anonymous healthy donor, resuspended (1×10^6/sample) in complete medium and incubated with IFNα2a (10 μg/mL), HA-IFNα2a (10 μg/mL in IFNα2a equivalent), HA 200 kDa (0.323 mg/mL; negative control), or left untreated for different times (5, 15, 30, and 60 min). At the end of treatments, the cells were fixed and permeabilized with Cytofix/Cytoperm Plus Kit (BD Biosciences, San Diego, USA), and finally labeled with a PE-conjugated mouse anti human Stat1 monoclonal antibody (mAb, BD Biosciences). Subsequently, similar experiments were performed with HCT-15 and SKOV-3 tumor cell lines at a single time point (60 min). All analyses were carried out using a flow cytometer FACS-Calibur (BD Biosciences) and the FlowJo 7.6.5 data analysis software package (TreeStar, USA).

2.9. RNA extraction, real-time PCR assay and gene expression profiling

Total RNA was extracted from PBMC treated with IFNα2a (10 μg/mL) or HA-IFNα2a (10 μg/mL in IFNα2a equivalent) for 6 h using RNeasy Mini Kit (QIAGEN, Hilden, Germany), following the manufacturer's specifications. RNA was quantified by UV spectrophotometer prior to convert into cDNA with RT^2 First Strand Kits (QIAGEN). Quantification of gene expression was performed by real-time quantitative RT-PCR (Gene Amp® 7700 sequence detection system, PerkinElmer), wherein primers and SYBR Green/Rox PCR master mix for IFNα2a-driven genes were synthesized as "assays-on-demand" by custom service of SABiosciences (QIAGEN). The expression of IFNα2a-guided genes in PBMC treated with the unconjugated or HA-conjugated cytokine was determined using the $2^{-\Delta\Delta Ct}$ method [33]. Fold change values of samples were determined using untreated PBMC as basal controls, after normalization with a pool of housekeeping genes as internal control reference (ACTB, B2M, GAPDH, HPRT1, and RPL113A).

2.10. Ethics statement

Procedures involving animals and their care were in conformity with Institutional Guidelines (D.L. 116/92 and subsequent implementing circulars), and experimental protocols (project ID: 3/2012) were approved by the local Ethical Committee of Padua University (CEASA). During *in vivo* experiments, animals in all experimental groups were examined daily for a decrease in physical activity and other signs of disease or drug toxicity; severely ill animals were euthanized by carbon dioxide overdose.

2.11. Mice

Six to eight week-old female severe combined immunodeficiency (SCID), and BALB/c nude mice were purchased from Charles River Laboratories (Calco, Italy), and housed in our Specific Pathogen Free (SPF) animal facility.

2.12. Preparation of IFNα2a- and HA-IFNα2a-Cy5.5, and optical imaging

To investigate the *in vivo* biodistribution of free or conjugated cytokine, IFNα2a and HA-IFNα2a conjugate were labeled with Cy5.5 dye following the protocol of Amersham CyDye™ (GE Healthcare Bio-Sciences AB, Uppsala, Sweden) protein labeling kit. The Cy5.5 in DMSO was added to the IFNα2a and HA-IFNα2a solutions, dissolved in 0.1 M phosphate buffer pH 8 using a molar ratio 5:1 of Dye NHS ester-to-IFNα2a. The conjugation reactions were performed at RT for 4 h with mild stirring. The resulting conjugates were purified chromatographically using a gel filtration column and a phosphate buffer as eluent. The products were concentrated and the buffer exchanged with PBS. The concentration of the dye was calculated at its absorption maximum of 694 nm. The molar absorption coefficient of Dye is 250,000 $M^{-1}\ cm^{-1}$ as reported by the manufacturer's data sheet. The absorbance of the conjugates at 280 nm was corrected for dye contribution, approximately the 18% of the absorbance at 694 nm. BALB/c nude and SCID mice were placed on a low manganese diet to reduce autofluorescence from normal mouse chow, and abdominal fur was removed by depilation where requested. Five days later, animals were injected i.p. or i.v. with Cy5.5-labeled IFNα2a (15 μg, 1 nm of dye) or HA-IFNα2a (15 μg in IFNα2a equivalent, 1 nm of dye). *In vivo* biodistribution was analyzed by total body scanning at different time points (0, 2, 4, 6, 24 h) on isoflurane/oxygen anesthetized animals, using the MX2 scanner (ART, Montreal, Canada). The

experiments were repeated three times. Moreover, to assess potential differences in biodistribution in tumor-bearing animals, the optical imaging analysis was also performed in mice carrying intraperitoneal OC induced by injection of PD-OVCA1 cells transduced with a lentiviral vector coding for the firefly luciferase reporter gene (luc), to track tumor growth [34].

2.13. Assessment of in vivo antitumor activity and survival analysis

SCID mice were inoculated i.p. with 3×10^6 PD-OVCA1 OC cells, or 5×10^6 HCT-15 CRC cells expressing high or low levels of CD44, at day 0. Pharmacological treatments were started at day 7 from cancer cell line injection and carried out according to a q7dx3 schedule. Each group of animals (n = 6 mice/group) received intraperitoneally HA-IFNα2a, IFNα2a, or was left untreated; in one experiment with PD-OVCA1, mice received 10 μg/injection of free or conjugated IFNα2a, while another assay was carried out with 1 μg/injection. Tumor growth and response to therapy were monitored by recording survival in PD-OVCA1-bearing mice, and by bioluminescence (BLI) analysis in HCT-15-carrying animals. In this latter case, images were acquired at different time points after *in vivo* cell injection using the IVIS Lumina II Imaging System (PerkinElmer). Specifically, ten minutes before each imaging session, animals were anesthetized with isoflurane/oxygen and administered i.p. with 150 mg/kg of D-luciferin (PerkinElmer) in DPBS. A constant region of interest (ROI) was manually selected around the abdomen of animals and the signal intensity was measured as radiance (ph/s/cm^2/sr) using the Living Image software 3.2 (PerkinElmer).

2.14. Biotolerability analysis and liver toxicity assessment

To evaluate the potential organ toxicity effects induced by bioconjugate or free cytokine after i.p. administration, SCID mice were injected once i.p. with 10 μg of free or conjugated IFNα2a (3 mice/group). At different time points thereafter (0, 8, 24, 48, and 72 h), mice sera were collected and alanine aminotranferase (ALT) and aspartate aminotransferase (AST) levels were determined using diagnostic kits (Sclavo Diagnostics, Siena, Italy). At day 3, animals were sacrificed and abdominal wall samples, liver, spleen, heart, kidneys and lungs were collected for histological analysis. Tissue specimens were fixed in 4% neutral-buffered formalin, embedded in paraffin, sectioned at 4 μm and stained with hematoxylin and eosin (H&E). Moreover, SCID mice inoculated i.p. with 10 μg/injection of free or conjugated cytokine according to a q7dx3 schedule, were weighed periodically throughout the experiment up to day 30, to evaluate the overall toxicity.

2.15. Statistical analysis

Survival curves and probabilities were estimated using the Kaplan-Meier technique. A log-rank test for comparisons or an ANOVA for repeated measures analysis of variance were used when required. Analyses of data were done using the MedCalc (version 12) and SigmaPlot (version 12.3) statistical packages.

3. Results

3.1. Synthesis and characterization of HA-IFNα2a

To generate a HA intermediate suitable for IFNα2a conjugation, aldehyde groups were grafted on the HA backbone by coupling an acetal spacer to the carboxylic groups of the polymer. This strategy has been previously reported [24]. To allow the preservation of HA backbone and the obtainment of a desired percentage of aldehyde groups, the exact degree of modification was calculated by ^{1}H NMR spectroscopy by comparing the integrations of the spacer's acetal group (1.10 ppm), and of the HA's acetyl group (1.85 ppm) signals. The HA-aldehyde synthesized for this study presented a degree of aldehyde modification of 4% mol. Thereafter, HA-acetal was activated to HA-aldehyde by a mild acid hydrolysis prior to selective *N*-terminal conjugation to IFNα2a. The time-course of IFNα2a coupling was monitored by size-exclusion chromatography (SEC). As expected, the disappearance of the peak of free protein ($t_R = 11.12$ min) over the time corresponded to the appearance of a new peak ($t_R = 5.49$ min) in agreement with the formation of the HA-IFNα2a conjugate, which has a higher hydrodynamic volume than IFNα2a (Fig. 1A). After an extensive dialysis, the purity of the product was checked by SEC to ensure the elimination of unreacted protein. The IFNα2a loading was 28% (w/w), and the reaction yield was 72%.

3.2. Characterization of HA-IFNα2a

To investigate if HAylation has produced variations on the tertiary structure of IFNα2a, CD analysis were conducted in near-UV (250–350 nm) region. As previously known, HA absorbs in the far-UV starting at 215 nm due to the carbohydrate units of the polymer that have an own absorbance, thus interfering with the IFNα2a spectra. In the near-UV range, 250–350 nm, the shape and the construct of the CD spectrum of a protein depends on the individual aromatic amino acid (Phe 250–270 nm, Tyr 270–290 nm, Trp 280–300 nm) and disulphide bonds (broad weak signals 250–350 nm), their mobility, the nature of their environment and their spatial disposition in the protein. So, near-UV CD was used in this case to study changes in the protein tertiary structure. IFNα2a, in its native conformation, with its 10 Phe, 5 Tyr and 2 Trp residues, showed two main negative minima at 292 nm and 286 nm (Fig. 1B). These bands, which indicate the existence of a defined tertiary structure, were assigned to the 2 Trp(s), suggesting that these two residues were also present in microenvironments of different asymmetries. The other minima in the spectra resulted from Phe, Tyr and disulphide bonds [35]. The spectrum of HA-IFNα2a showed a similar trend in all the regions, thus indicating that the tertiary protein structure was preserved. In particular, the two main negative minima were almost superimposable suggesting that also the microenvironment surrounding these residues was unchanged.

3.3. Identification of HAylation site of HA-IFNα2a

To confirm the site of conjugation of IFNα2a, a peptide mapping analysis was performed using trypsin as proteolytic enzyme. The tryptic digests were analyzed by RP-HPLC (Fig. S1). The protein sequence coverage was about 95%, for both samples. Each peak, matching a peptide fragment, was compared between the native and HAylated IFNα2a digests in the RP-HPLC elution profile (Fig. S1), and the corresponding molecular mass was obtained by ESI-TOF (Table S1). The masses of all peptide fragments of native and conjugated IFNα2a were determined experimentally and were very similar to the theoretical expected values (Table S1). Almost all the native IFNα2a tryptic fragments containing lysines were identified, except the dipeptide E_{132}–K_{133}, which is located between two cleavage sites, K131 and K134 (ITLYLK$_{131}$EK$_{133}$K$_{134}$YSPCAWEVVR). Nevertheless, it is important to highlight that whether HA was coupled to one of such lysine, the cleavage by trypsin would be strongly hampered by the steric entanglement of the polymer. Also, the last lysine at the C-terminus (K164) was not identified because trypsin cuts after R162, thus forming a small tripeptide, SKE, which could not be determined. Since the peptide F13 [150–163] was fully identified in both native and HAylated IFNα2a, it is conceivable that also in this case, if HA was coupled to K164, trypsin would not be able to cut after R163 owing to the steric hindrance. The main difference between the two samples is the peak eluted at 9.7 min, with a mass of 1369.6267 Da. The peak corresponds to the *N*-terminal IFNα2a fragment (F1), which was not detected in the digested RP profile of HA-IFNα2a; no other peaks with the same molecular weight were identified by mass analysis for HAylated IFNα2a. After the *N*-terminal conjugation of IFNα2a with HA, the HAylated fragment could not be detected by ESI-TOF, indicating that the α-amino group at the *N*-terminus was selectively coupled to HA.

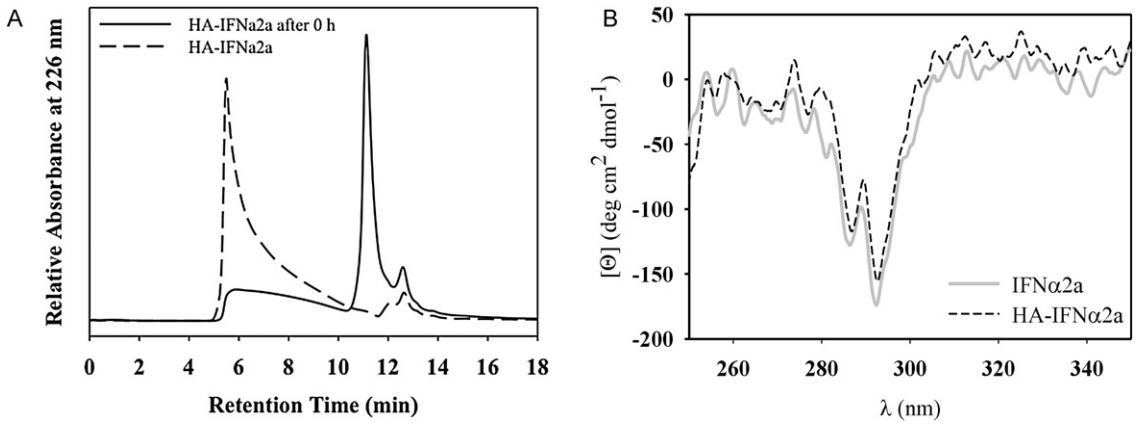

Fig. 1. Reaction and characterization of HA-IFNα2a. (A) Elution profiles of HA-IFNα2a and IFNα2a in SEC-HPLC. The peak of IFNα2a (solid line) appeared at 11.125 min, whereas the elution profiles of the HA-conjugated cytokine (dotted line) disclosed a new peak at 5.495 min. (B) Comparison of the tertiary structure of native IFNα2a and HA-IFNα2a by near-UV CD. As outlined in the experimental procedures, the spectra were recorded at the protein concentration of 1 mg/mL. The analysis demonstrated that HAylated IFNα2a (dotted line) preserved the tertiary structure of native IFNα2a (grey line).

3.4. Antiviral activity of HA-IFNα2a

To assess whether IFNα2a was still functional upon conjugation with HA, a test of antiviral activity was performed using the free or conjugated cytokine. To this end, VERO cells were pretreated with scalar doses of IFNα2a, HA-IFNα2a or HA for 24 h to induce the antiviral state, followed by infection with the cytopathic vesicular stomatitis virus (VSV), and assessment of cell viability the day after. IFNα2a treatment before VSV infection induced in VERO cells a strong resistance to the cytopathic effects of the virus, with an $IC_{50} \pm$ S.E. of 0.351 ± 0.067 μg/mL (Fig. 2A and B). Notably, the HA-conjugated cytokine maintained a relevant antiviral effect that was only 2.4-fold (0.828 ± 0.108 μg/mL) lower than that exhibited by IFNα2a, thus demonstrating that the biological activity of the molecule was impaired only in part by conjugation to HA (Fig. 2A and B). Moreover, the antiviral activity had to be ascribed only to the conjugated cytokine, as the 200 kDa HA carrier was devoid of any effect, leading all cells to succumb the cytopathic effects of virus infection (Fig. 2A and B).

3.5. Antiproliferative activity of HA-IFNα2a

IFNα2a is well known to exert a powerful antiproliferative activity, which is however highly variable depending on the cell type [36]. To identify potential suitable targets to focus on, we initially tested a panel of ovarian and colorectal cancer cell lines for both CD44 expression (Fig. S2) and susceptibility to IFNα2a, wherein the cells were incubated with two screening concentrations of the cytokine (0.05 ng/mL and 0.5 μg/mL), and then assessed for viability. As shown in Fig. 2C, three cell lines resulted sensitive to the antiproliferative activity of the cytokine, namely the HCT-15 colorectal adenocarcinoma, and the SKOV-3 and PD-OVCA1 ovarian tumors; in particular, this latter was completely inhibited by the higher dose of IFNα2a. Subsequently, both the HCT-15 and the PD-OVCA1 cell lines underwent titration experiments with the free or conjugated cytokine, and the HA carrier as control (Fig. 2D). Results showed that IFNα2a induced a dose-dependent growth inhibition activity in both cell lines, with a $IC_{50} \pm$ S.E. of 0.188 ± 0.028 μg/mL and 0.0003 ± 0.0001 μg/mL for HCT-15 and PD-OVCA1, respectively. While the HA carrier had no effect, the bioconjugate also disclosed a dose-dependent growth inhibition, being the $IC_{50} \pm$ S.E. for HCT-15 and PD-OVCA1 of 0.99 ± 0.263 μg/mL and 0.079 ± 0.026 μg/mL, respectively. Overall, the results of both the antiviral and antiproliferative experiments indicate that IFNα2a conjugation to HA reduces but not abrogate the biological activity of the cytokine.

3.6. Signaling pathway of HA-IFNα2a

The IFN signaling pathway mainly involves the phosphorylation of the tyrosine residues of Janus kinase (JAK) and signal transducers and activators of transcription (STAT) proteins. This is the pivotal mechanism leading to interferon-inducible gene expression [2]. A very upstream step critical for IFNα2a signaling *via* the JAK-STAT pathway is the phosphorylation of STAT1 tyrosine 701 residue (pSTAT1), which can be determined by a simple cytometry analysis with a specific mAb [4]. Therefore, to assess the phosphorylation state of STAT1 upon incubation of responsive cells with the free or conjugated cytokine, PBMC isolated from anonymous healthy donor were incubated with IFNα2a, HA-IFNα2a, HA, or left untreated. At different time points thereafter, cells were fixed and permeabilized, and finally labeled with the anti-pSTAT1 mAb. PBMC left untreated or treated with HA did not present STAT1 phosphorylation; conversely, HA-IFNα2a treatment induced a marked phosphorylation of the protein at levels comparable to those observable using the free cytokine (Fig. 3A). Analysis of fluorescence intensity at the different time points tested disclosed that STAT1 phosphorylation in PBMC raised very rapidly, to remain constant thereafter. Subsequently, similar experiments were performed on HCT-15 and SKOV-3 tumor cell lines at a representative time point of 60 min. Results of flow cytometry analysis showed that both HA-IFNα2a and IFNα2a induced similar levels of STAT1 phosphorylation (Fig. 3B).

3.7. Gene signature of IFNα2a and HA-IFNα2a in responding cells

Stimulation with IFNα2a is known to induce a well-defined gene signature [37]. To evaluate whether the bioconjugate retained similar properties, PBMC isolated from anonymous healthy donor were stimulated with HA-IFNα2a or the free cytokine, and the expression of IFNα2a-stimulated genes was assessed by quantitative RT-PCR assay. A set of 84 IFNα2a-inducible genes were analyzed, and resulted similarly expressed (Fig. 3C), as also indicated by the marked correlation between the ΔΔCt values obtained in the two experimental conditions (Fig. 3C, inset). Such results further strength the concept that conjugation to HA did not substantially alter IFNα2a activity pattern: indeed, only 5 out of the 84 IFN-induced genes tested were differentially regulated by the conjugated cytokine, as compared to the free form.

3.8. Assessment of in vivo biodistribution of HA-IFNα2a

Initially, *in vivo* biodistribution of either Cy5.5-labeled IFNα2a and HA-IFNα2a was assessed by optical imaging following both i.v. and i.p.

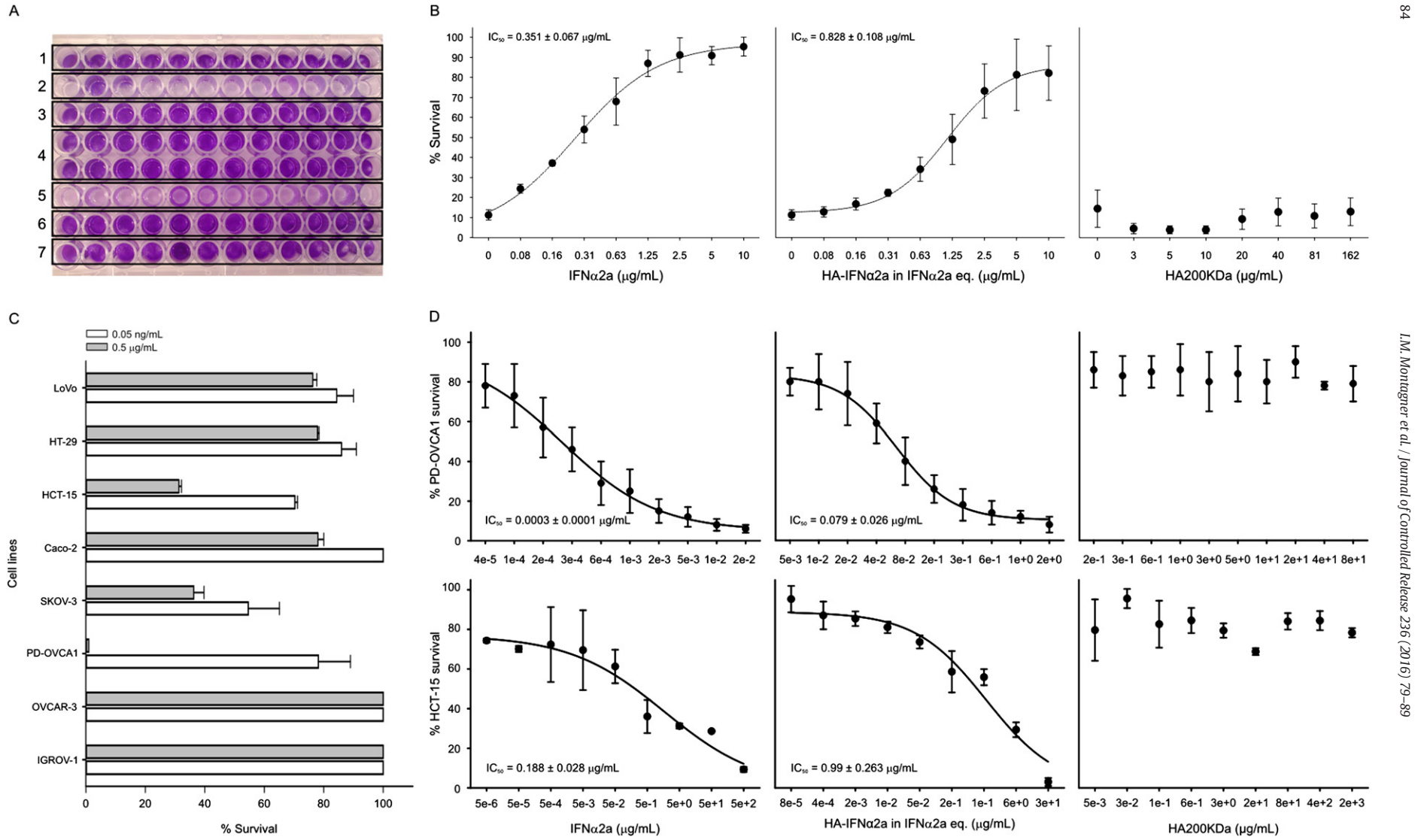

Fig. 2. IFNα2a-induced antiviral effects in VERO cells, and antiproliferative activity against different tumor cell lines. (A) Photograph of a microplate with VERO cells treated with free or conjugated cytokine, and stained with crystal violet. Row 1, untreated cells; row 2, cells infected with VSV; row 3, cells incubated with IFNα2a and infected with VSV; rows 4, cells incubated with HA-IFNα2a and infected with VSV; row 5, cells incubated with HA 200 kDa and infected with VSV; row 6, cells incubated with IFNα2a; row 7, cells incubated with HA 200 kDa. (B) Cells were incubated with escalating concentrations of IFNα2a, HA-IFNα2a or HA 200 kDa (negative control), infected with VSV 24 h later, and finally assessed for viability by the ATPlite assay. The values of IC_{50} reported are the mean ± S.E. of four viability experiments. For each experiment, the IC_{50} was calculated from each single semi-logarithmic dose-response curve by linear interpolation, and obtained values were then averaged. Values are reported in μg/mL, and for the bioconjugate they are expressed in terms of free drug equivalents. (C) Human colorectal (LoVo, HT-29, HCT-15 and Caco-2) and ovarian (SKOV-3, PD-OVCA1, OVCAR-3 and IGROV-1) cancer cell lines were screened for susceptibility to IFNα2a by incubation with a high (0.5 μg/mL) and low (0.05 ng/mL) concentration of the cytokine, and the resulting growth inhibition was evaluated by the ATPlite assay. To note, data reported for the HCT-15 tumor cell line refer to an unselected population with ~20% of CD44 expression (Fig. S2). (D) The cytotoxicity induced by escalating doses of IFNα2a, HA-IFNα2a or HA 200 kDa was finally studied in depth in the more IFNα2a-susceptible cell lines PD-OVCA1 and HCT-15, representative of the ovarian and colorectal tumor histotypes, respectively. The values of IC_{50} reported in μg/mL are the mean ± S.E. of five viability experiments carried out for each tumor cell line.

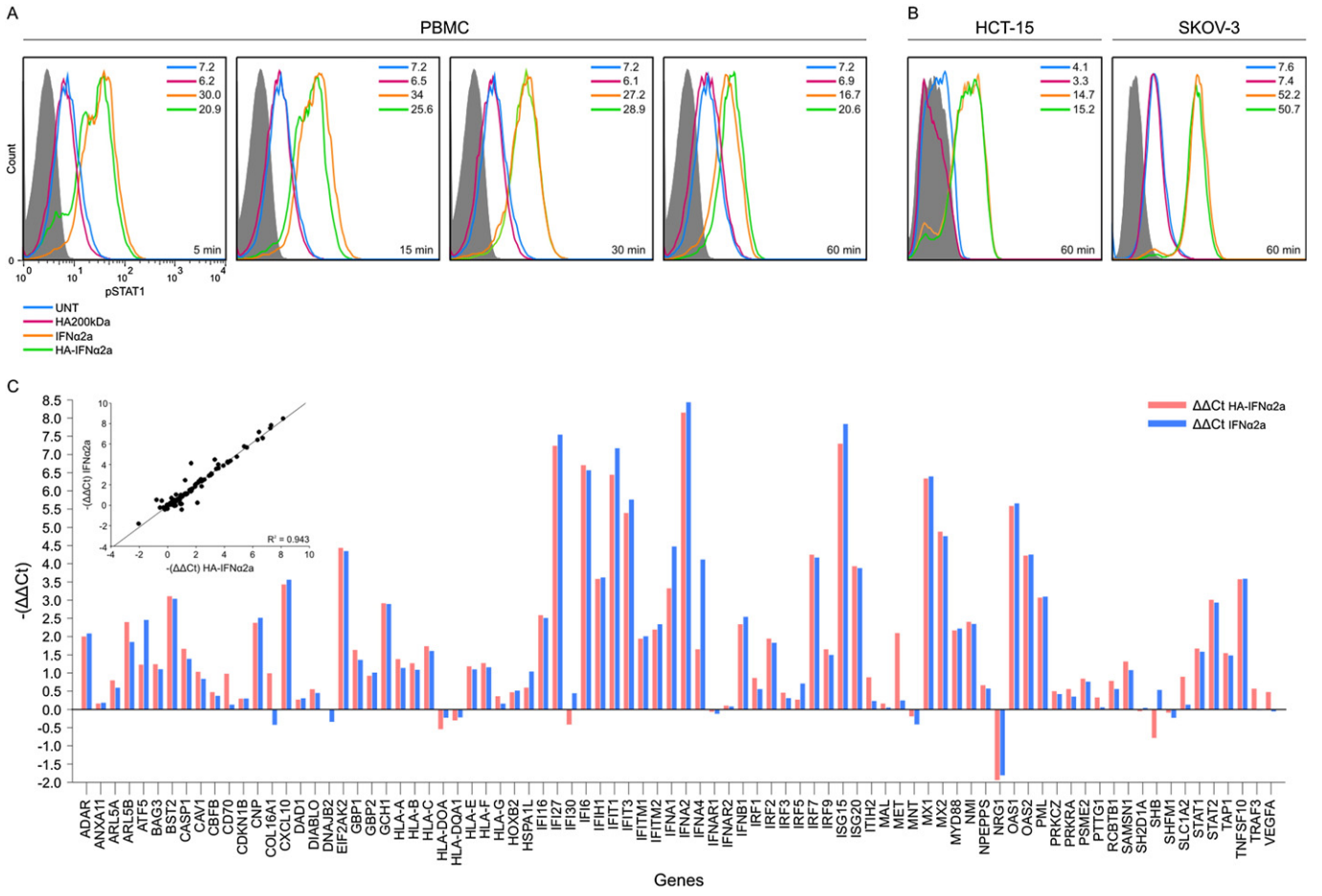

Fig. 3. Analysis of STAT1 phosphorylation, and IFNα2a-inducible gene expression signature in PBMC. (A) PBMC were treated with IFNα2a (orange), HA-IFNα2a (green), HA 200 kDa (red) or left untreated (blue) for different times (5, 15, 30, and 60 min), fixed, permeabilized, and stained with a PE-labeled mouse anti human pSTAT1 mAb. (B) HCT-15 and SKOV-3 tumor cell lines were incubated with the compounds as in A, for 1 h and stained as above. Both in A and B, grey plots depict the isotype control, while data at the upper-right corner of each panel report geo-mean values. (C) Quantitative RT-PCR analysis of 84 selected IFNα2a-inducible genes in PBMC treated with free (blue) or HA-conjugated IFNα2a (red). Wilcoxon Signed Rank Test P = 0.119. The graph at the upper-left corner is a scatter plot depicting the correlation in the ΔΔCt values between PBMC treated with free or HA-conjugated IFNα2a, as assessed by RT-PCR. The correlation coefficient (R) is reported at the bottom of the panel.

administration in healthy mice. With regard the i.v. route, results disclosed a rapid liver targeting of the bioconjugate as compared to the free cytokine, thus essentially confirming previously reported data [38]. Indeed, an almost complete preferential liver accumulation of HA-IFNα2a was already observable 2 h after administration, and lasted up to 24 h; conversely, the fluorescence signal from the free cytokine rapidly disappeared and concentrated in the bladder, thus suggesting a potential renal clearance (Fig. 4A). Histograms reported in Fig. 4B show the percentage of total photons emitted from the ROI around the liver respect to the total body emission, and clearly disclose a different kinetics of liver accumulation between the two compounds (P = 0.002). When the biodistribution of Cy5.5-labeled IFNα2a and HA-IFNα2a was studied upon i.p. administration, total body scanning disclosed that the HA-conjugated and free cytokine again presented different kinetics and patterns of biodistribution (Fig. 4C). Indeed, HA-IFNα2a produced a signal that remained confined to the peritoneal cavity much longer than the free cytokine, with an emission peak at 2 h post-injection, and a decrease only at 24 h after administration. On the contrary, the signal of the free cytokine disappeared very rapidly. Indeed, histograms reported in Fig. 4D and showing the percentage of total photons emitted from ROI around the peritoneal cavity, clearly evidence a different kinetics of permanence between the two compounds (P = 0.001). To confirm such data also in cancer-bearing animals at an advanced stage of disease, biodistribution experiments were repeated in mice with a hemorrhagic and ascitic PD-OVCA1 tumor (Fig. S4). Even in this case, kinetics and patterns of biodistribution appeared different in mice receiving either the free or bound cytokine (Fig. 4E and F, P = 0.004), although the total photon fluxes in both groups were reduced, likely due to the quenching activity of haemoglobin in ascites [39]. Thus, HA-IFNα2a appears to act as a depot formulation that improves the bioavailability of the cytokine in the peritoneum.

3.9. In vivo therapeutic activity of HA-IFNα2a

Before assessing the *in vivo* therapeutic efficacy of HA-IFNα2a against OC, additional experiments were carried out with the HCT-15 CRC cell line, which had showed to be slightly sensitive to IFNα2a (Fig. 2C). This was done with a double purpose: on one hand, to directly evaluate the antitumor activity *in vivo* of the free and bound cytokine, and on the other hand to gain insight about the potential relevance of CD44 as target of the HA carrier moiety. Indeed, HCT-15 was the only tumor cell line among those tested that allowed the isolation of two subpopulations having a high and low expression of the receptor. Therefore, SCID mice were inoculated i.p. with HCT-15 $CD44^{low}$ or HCT-15 $CD44^{high}$ cell lines, and treated locally with 10 μg/injection (q7dx3 schedule) of free or HA-conjugate IFNα2a. The therapeutic impact of the different treatments was evaluated by BLI, as the total photon flux is strictly correlated with tumor growth [40]. As illustrated in Fig. 5A, HA-IFNα2a significantly restrained the growth of HCT-15 $CD44^{high}$ tumors, while the free cytokine had no effect. Conversely, in

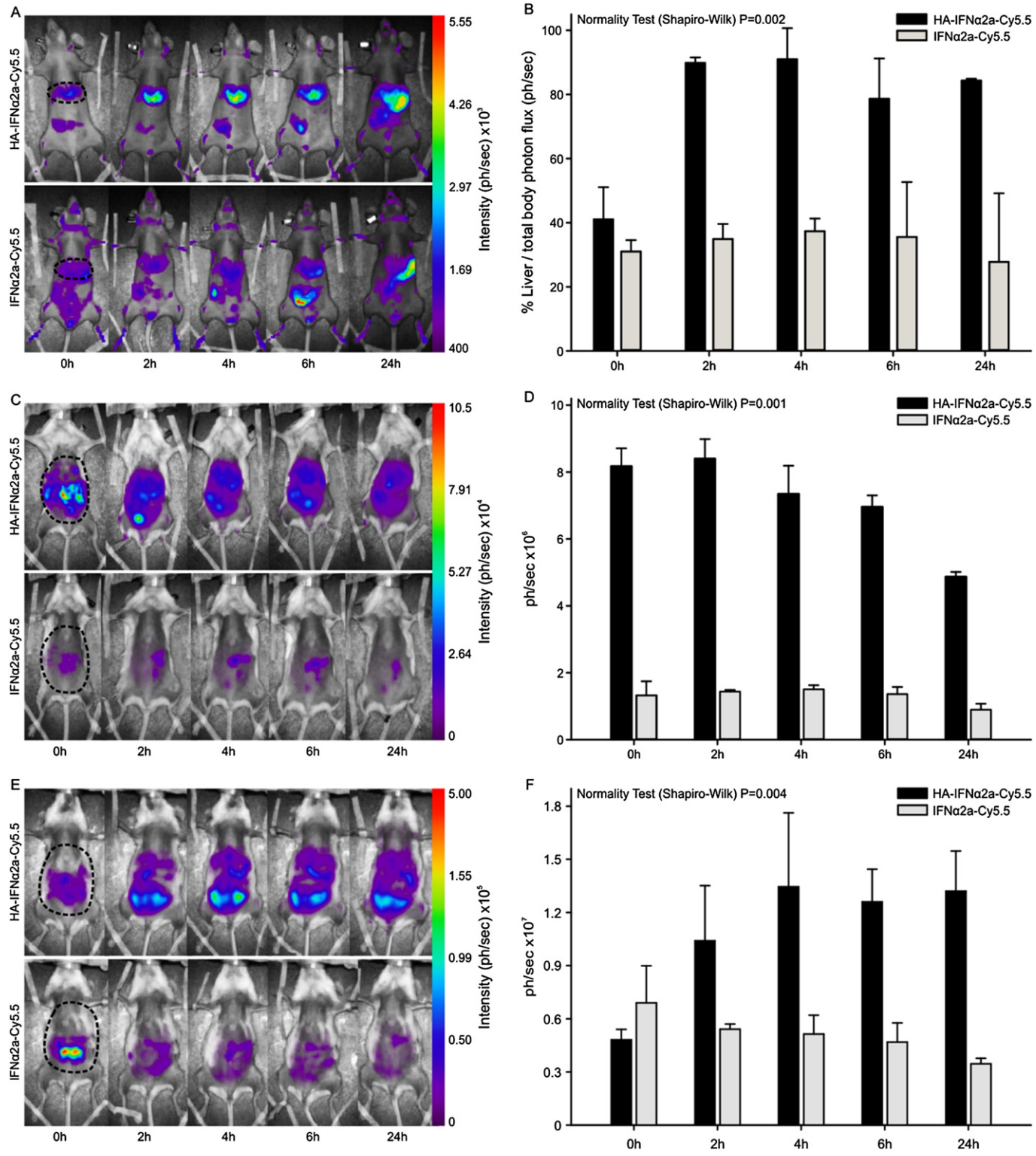

Fig. 4. Biodistribution analysis of Cy5.5-labeled HA-IFNα2a and IFNα2a in BALB/c nude and SCID mice. (A) BALB/c nude mice were injected i.v. with Cy5.5-labeled HA-IFNα2a (upper panels) or IFNα2a (lower panels). Biodistribution kinetics of the compounds was assessed by fluorescence optical imaging as total body scanning with a 670 nm laser and a 693LP filter; spatial resolution/scan step was fixed at 1.5 mm, exposure time was 0.5 s, and laser power was automatically adjusted for each scan session. The figure shows one representative experiment of three that produced similar results. (B) The vertical histograms represent the percentage of total photons emitted from ROI around the liver respect to the total body emission. Data are expressed as photon flux and quantified as photon × second^{-1}. Three mice per group were analyzed and data are reported as mean ± S.D. (C) SCID mice were injected i.p. with Cy5.5-labeled HA-IFNα2a (upper panels) or IFNα2a (lower panels). Biodistribution kinetics of the compounds was assessed as reported in (A). (D) The vertical histograms refer to the total photons emission from mouse abdominal ROI. Data and mice as in (B). (E) Experiments and data analysis shown in (C) and (D) were repeated in mice bearing an ascitic PD-OVCA1 tumor (Fig. S3).

mice injected with the cell line expressing low levels of the receptor nor the HA-IFNα2a or IFNα2a produced a therapeutic benefit (Fig. 5B). As a confirmation, the therapeutic activity of free and bound cytokine was also evaluated in an OC model induced by the i.p. injection of PD-OVCA1 tumor cells. In a first experiment, mice were treated locally with 10 μg/injection (q7dx3 schedule) of free or HA-conjugated

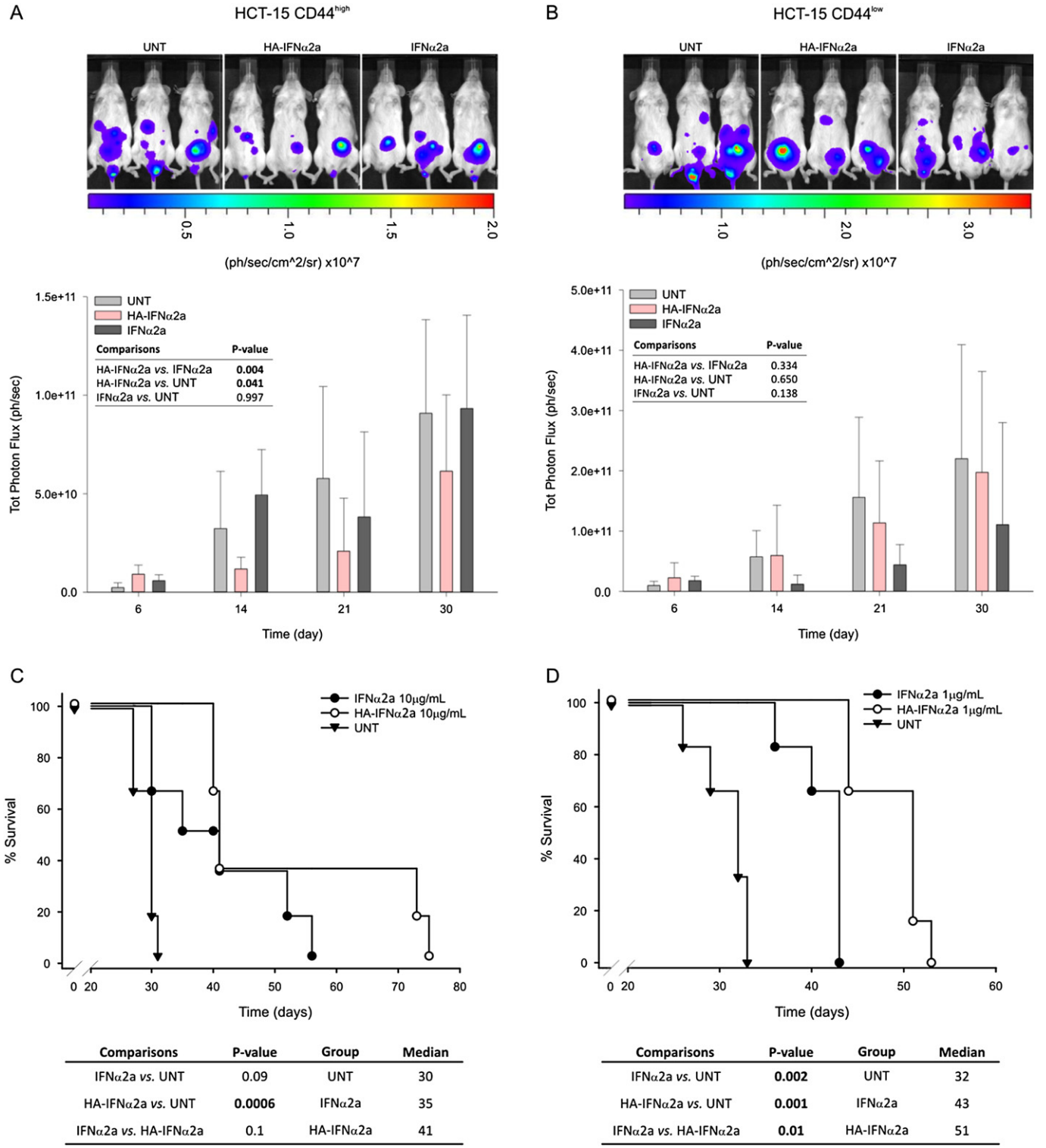

Comparisons	P-value	Group	Median
IFNα2a *vs.* UNT	0.09	UNT	30
HA-IFNα2a *vs.* UNT	**0.0006**	IFNα2a	35
IFNα2a *vs.* HA-IFNα2a	0.1	HA-IFNα2a	41

Comparisons	P-value	Group	Median
IFNα2a *vs.* UNT	**0.002**	UNT	32
HA-IFNα2a *vs.* UNT	**0.001**	IFNα2a	43
IFNα2a *vs.* HA-IFNα2a	**0.01**	HA-IFNα2a	51

Fig. 5. *In vivo* IFNα2a antitumor activity. (A) and (B) BLI of mice inoculated with 5×10^6 bioluminescent (A) HCT-15 CD44^{high} or (B) HCT-15 CD44^{low} cells, and treated with 10 μg/injection (q7dx3 schedule) of IFNα2a, HA-IFNα2a (in IFNα2a equivalents), or left untreated (UNT). Panels show three representative mice/group 30 days after tumor injection. Under each panel, the vertical plot reports the cumulative total photons emission at different time points (6, 14, 21, 30 days). Six mice per group were analyzed, and data represent means ± SD. Statistical analysis: ANOVA for repeated measures analysis of variance. (C) and (D) Kaplan-Meier survival curves of PD-OVCA1-bearing mice treated with 10 μg/injection or 1 μg/injection, respectively, of IFNα2a, HA-IFNα2a (in IFNα2a equivalents) or left untreated (UNT). In both cases, the administration schedule was q7dx3. Statistical analysis and median survival time are reported in table at the bottom of each panel.

IFNα2a through the i.p. route. Results of Fig. 5C show that HA-IFNα2a loco-regional treatment (median survival, 41 day) evidenced a relevant growth inhibitory effect and induced an increased survival compared to untreated mice (median survival, 30 day; P = 0.0006). Although the HA-IFNα2a led to a higher survival compared to free cytokine (median survival, 35 day), data did not reach a statistical significance (P = 0.1). Therefore, to highlight the targeting properties of the bioconjugate a second experiment was carried out, where 10-fold less (1 μg/injection, q7dx3 schedule) of free or bound cytokine was administered (Fig. 5D). Results showed that PD-OVCA1-bearing mice treated with HA-IFNα2a

(median survival, 51 day) exhibited an increased survival compared to both untreated control mice (median survival, 32 day; $P = 0.002$) and free IFNα2a-treated mice (median survival, 43 day; $P = 0.01$)

3.10. Biotolerability and liver toxicity analysis

In a clinical setting, locally administered antitumor therapies must be well tolerated. To assess whether the free or bound forms of the cytokine induced toxic effects on the mesothelial lining and peritoneal organs, three groups of SCID mice were injected once i.p. with the bioconjugate or free IFNα2a. Full thickness specimens of the abdominal wall, and liver, spleen, heart, kidneys and lungs were collected at day 3 after treatment, and analyzed histologically. All samples did not show inflammatory infiltrates or morphological alterations (Fig. S4), even in the case of HA-IFNα2a administration, where the cytokine persist longer in the peritoneal cavity. Moreover, AST and ALT liver enzymes activity in the plasma of treated mice turned out to be under the detection threshold level of the diagnostic kits employed, thus indicating the absence of direct liver toxicity (data not show). Additionally, for the assessment of overall toxicity SCID mice were treated with bioconjugate or free cytokine according to a q7dx3 schedule, and the weight was periodically recorded over a 1-month period. No weight loss was observed, nor differences in average body weight between treated and untreated mice (Fig. S5).

4. Discussion

OC imperatively needs new treatment modalities because at present there are no decisive therapeutic solutions. This condition could benefit of a targeted therapy, because the peritoneum-plasma barrier can allow a local delivery of drugs, thus potentially reducing heavy systemic side effects.

Here, we took advantage of our expertise in HA-based bioconjugates to improve also the direct delivery of IFNα2a to the peritoneal cavity. This strategy has the potentiality to improve the treatment of OC, in particular in terms of safety and tolerability. Indeed, we previously showed that the loco-regional administration of a paclitaxel-HA conjugate outperformed the free drug in terms of tolerability and therapeutic efficacy in an OC preclinical setting [27]. In addition, the bioconjugate was also very efficient towards different models of peritoneal carcinomatosis [26], and bladder cancer both in experimental [25] and clinical conditions [41]. Moreover, another HA bioconjugate (SN38-HA) has been successfully tested in a mouse model of CRC peritoneal carcinomatosis [42] and OC [43]. Therefore, HA can act as a suitable carrier being endowed with the capability to selectively target tumor cells through the binding to CD44. This receptor is over-expressed in many cancers, including the ovarian histotype as exemplified by cytometry results outlined in this work and previously [26,43]. Moreover, it has been shown that HA has *per se* the capacity to reduce postoperative and disease-related adhesions without impacting the metastatic potential of tumor cells [44]. In addition, it can exert a relevant depot effect [45,46]. In the case of HA conjugation to proteins, it is mandatory to exploit a site-selective conjugation approach to avoid the risk of cross-linking. In this regards, an innovative HA-aldehyde was previously designed and studied for yielding a site-selective *N*-terminus protein [24].

Remarkably, the conjugate maintained the anti-viral and anti-proliferative activities of the free cytokine. In addition, the JAK-STAT signaling pathway was similarly activated by the free and bound form of IFNα2a, while the gene expression profile induced by HA-IFNα2a slightly diverged for only 5 out of the 84 genes activated by the free cytokine, thus suggesting a substantially identical pattern of gene mobilization. Moreover, the preserved pleiotropic activities of the cytokine were implemented by the intrinsic targeting properties of HA. The *in vivo* biodistribution and fate of HA-IFNα2a differed from that of IFNα2a, and was dictated by the hyaluronan moiety both in healthy and tumor-bearing mice. Indeed, i.p.-injected HA-IFNα2a remained into the peritoneal cavity longer than IFNα2a. This kind of "depot effect" ensures a prolonged cytokine release without inducing local adverse reactions, as shown by the lack of histological alterations in intraperitoneal and peripheral organs. In this regard, we previously demonstrated that HA-bioconjugates are absolutely devoid of any proinflammatory [27]. The improved bioavailability and the targeting properties of the HA-IFNα2a conjugate entailed an enhanced therapeutic efficacy, as demonstrated in the proof-of-principle therapeutic experiment involving CRC subpopulations expressing high or low levels of CD44 receptor. The lack of therapeutic benefit of both the free and conjugated cytokine against HCT-15 $CD44^{low}$ tumors in conjunction with the efficacy of the HA-IFNα2a against HCT-15 $CD44^{high}$ counterparts, incontrovertibly supports the notion that HA-mediated retargeting of CD44 can make effective a cytokine otherwise devoid of therapeutic impact. Accordingly, in OC xenograft mouse models the HA-IFNα2a bioconjugate significantly prolonged mice long-term survival with respect to the free cytokine. In particular, this improved therapeutic effect was evidenced with the lowest dose of cytokine, as a proof-of-concept of the fine targeting capacity of the HA moiety. Conversely, due to the great sensitivity of PD-OVCA1 cells to the cytokine, the administration of HA-IFNα2a and IFNα2a at high dose completely abrogated any difference in the treatment outcome.

While not relevant for OC treatment, for the sake of completeness the biodistribution of the bioconjugate given i.v. was also investigated. As previously demonstrated [38], i.v.-injected bioconjugate disclosed a marked accumulation in the liver, mainly due to the presence of the HARE receptors in this district [47], and was not toxic. Because of this peculiar accumulation of the i.v.-administered HA-IFNα2a, the bioconjugate can be envisaged also as a safe and targeted treatment for liver diseases, especially HBV or HCV infections.

Overall, present data envisage that the conjugation of IFNα2a to HA can provide an effective strategy to improve the loco-regional treatment of OC, thus supporting its further testing in a clinical setting.

5. Conclusion

This study demonstrated that the site-selective conjugation of IFNα2a with HA resulted in the construction of an efficient therapeutic agent for OC treatment. Several tests demonstrated that HA-IFNα2a preserved the protein activity thanks to precise conjugation chemistry based on the use of a HA-aldehyde derivative. The conjugation allowed to confine the drug to the peritoneal cavity, thus acting as a depot formulation that improved the bioavailability of the cytokine in the peritoneum. In the xenograft mouse models, HA-IFNα2a exhibited a superior antitumor activity in comparison to the free cytokine. These results confirm that the project's aim was achieved and encourage further investigations.

Acknowledgements

GP and AR were partly supported by the Italian Association for Cancer Research (AIRC; MFAG #15458, IG-17035 and Special Program Molecular Clinical Oncology 5 per mille ID 10016) and by the Italian Ministry of Health (Ricerca Finalizzata GR-2011-02351128).

Appendix A. Supplementary data

Supplementary data to this article can be found online at http://dx.doi.org/10.1016/j.jconrel.2016.06.033.

References

[1] S. Pestka, C.D. Krause, M.R. Walter, Interferons, interferon-like cytokines, and their receptors, Immunol. Rev. 202 (2004) 8–32.
[2] A.H. van Boxel-Dezaire, M.R. Rani, G.R. Stark, Complex modulation of cell type-specific signaling in response to type I interferons, Immunity 25 (2006) 361–372.
[3] G.R. Stark, I.M. Kerr, B.R. Williams, R.H. Silverman, R.D. Schreiber, How cells respond to interferons, Annu. Rev. Biochem. 67 (1998) 227–264.

[4] C. Schindler, C. Plumlee, Inteferons pen the JAK-STAT pathway, Semin. Cell Dev. Biol. 19 (2008) 311–318.
[5] F.C. Lin, H.A. Young, Interferons: success in anti-viral immunotherapy, Cytokine Growth Factor Rev. 25 (2014) 369–376.
[6] L. Cha, C.M. Berry, D. Nolan, A. Castley, S. Fernandez, M.A. French, Interferon-alpha, immune activation and immune dysfunction in treated HIV infection, Clin. Transl. Immunology. 3 (2014), e10.
[7] N.G. Gavalas, A. Karadimou, M.A. Dimopoulos, A. Bamias, Immune response in ovarian cancer: how is the immune system involved in prognosis and therapy: potential for treatment utilization, Clin. Dev. Immunol. 2010 (2010) 791603.
[8] K. Kaur, P. Kush, R.S. Pandey, J. Madan, U.K. Jain, O.P. Katare, Stealth lipid coated aquasomes bearing recombinant human interferon-alpha-2b offered prolonged release and enhanced cytotoxicity in ovarian cancer cells, Biomed. Pharmacother. 69 (2015) 267–276.
[9] I. Gresser, The antitumor effects of interferon: a personal history, Biochimie 89 (2007) 723–728.
[10] K.P. Kotredes, A.M. Gamero, Interferons as inducers of apoptosis in malignant cells, J. Interf. Cytokine Res. 33 (2013) 162–170.
[11] F. Fabrizi, V. Dixit, P. Messa, Interferon mono-therapy for symptomatic HCV-associated mixed cryoglobulinemia: meta-analysis of clinical studies, Acta Gastroenterol. Belg. 76 (2013) 363–371.
[12] M. Ferrantini, I. Capone, F. Belardelli, Interferon-alpha and cancer: mechanisms of action and new perspectives of clinical use, Biochimie 89 (2007) 884–893.
[13] E.R. Plimack, J.R. Desai, J.P. Issa, J. Jelinek, P. Sharma, L.M. Vence, R.L. Bassett, J.L. Ilagan, N.E. Papadopoulos, W.J. Hwu, A phase I study of decitabine with pegylated interferon alpha-2b in advanced melanoma: impact on DNA methylation and lymphocyte populations, Investig. New Drugs 32 (2014) 969–975.
[14] I. Rouanet, C. Lechiche, R. Doncesco, J.M. Mauboussin, A. Sotto, Interferon therapy for Kaposi sarcoma associated with acquired immunodeficiency syndrome: still a valid treatment option? AIDS Patient Care STDs 27 (2013) 537–538.
[15] R. Passalacqua, C. Caminiti, S. Buti, C. Porta, R. Camisa, L. Braglia, G. Tomasello, A. Vaglio, R. Labianca, E. Rondini, R. Sabbatini, G. Nastasi, F. Artioli, A. Prati, M. Potenzoni, D. Pezzuolo, E. Oliva, F. Alberici, C. Buzio, POLAR-01 Trial Investigators, adjuvant low-dose interleukin-2 (IL-2) plus interferon-alpha (IFN-alpha) in operable renal cell carcinoma (RCC): a phase III, randomized, multicentre trial of the Italian Oncology Group for Clinical Research (GOIRC), J. Immunother. 37 (2014) 440–447.
[16] J. Zhou, Advances and prospects in cancer immunotherapy, New J. Sci. 2014 (2014).
[17] C. Marth, G.H. Windbichler, H. Hausmaninger, E. Petru, K. Estermann, A. Pelzer, E. Mueller-Holzner, Interferon-gamma in combination with carboplatin and paclitaxel as a safe and effective first-line treatment option for advanced ovarian cancer: results of a phase I/II study, Int. J. Gynecol. Cancer 16 (2006) 1522–1528.
[18] L. Capuron, A.H. Miller, Cytokines and psychopathology: lessons from interferon-alpha, Biol. Psychiatry 56 (2004) 819–824.
[19] H. Orlent, B. Hansen, H.L. Janssen, R.J. De Knegt, High-dose (peg)interferon therapy in treatment-naive, interleukin-28B rs12979860 CT/TT genotype 1 chronic hepatitis C, Dig. Liver Dis. 47 (2015) 87–88.
[20] N. Miyakawa, M. Nishikawa, Y. Takahashi, M. Ando, M. Misaka, Y. Watanabe, Y. Takakura, Prolonged circulation half-life of interferon gamma activity by gene delivery of interferon gamma-serum albumin fusion protein in mice, J. Pharm. Sci. 100 (2011) 2350–2357.
[21] Z. Li, L. Li, Y. Liu, H. Zhang, X. Li, F. Luo, X. Mei, Development of interferon alpha-2b microspheres with constant release, Int. J. Pharm. 410 (2011) 48–53.
[22] M. Gulia, S. Rai, U.K. Jain, O.P. Katare, A. Katyal, J. Madan, Sustained-release protamine sulphate-impregnated microspheres may reduce the frequent administration of recombinant interferon alpha-2b in ovarian cancer: in-vitro characterization, Anti-Cancer Drugs 25 (2014) 63–71.
[23] A. Mero, M. Campisi, M. Caputo, C. Cuppari, A. Rosato, O. Schiavon, G. Pasut, Hyaluronic acid as a protein polymeric carrier: an overview and a report on human growth hormone, Curr. Drug Targets 16 (2015) 1503–1511.
[24] A. Mero, M. Pasqualin, M. Campisi, D. Renier, G. Pasut, Conjugation of hyaluronan to proteins, Carbohydr. Polym. 92 (2013) 2163–2170.
[25] I.M. Montagner, A. Banzato, G. Zuccolotto, D. Renier, M. Campisi, P. Bassi, P. Zanovello, A. Rosato, Paclitaxel-hyaluronan hydrosoluble bioconjugate: mechanism of action in human bladder cancer cell lines, Urol. Oncol. 31 (2013) 1261–1269.
[26] I.M. Montagner, A. Merlo, G. Zuccolotto, D. Renier, M. Campisi, G. Pasut, P. Zanovello, A. Rosato, Peritoneal tumor carcinomatosis: pharmacological targeting with hyaluronan-based bioconjugates overcomes therapeutic indications of current drugs, PLoS One 9 (2014), e112240.
[27] A. Banzato, S. Bobisse, M. Rondina, D. Renier, F. Bettella, G. Esposito, L. Quintieri, L. Melendez-Alafort, U. Mazzi, P. Zanovello, A. Rosato, A paclitaxel-hyaluronan bioconjugate targeting ovarian cancer affords a potent in vivo therapeutic activity, Clin. Cancer Res. 14 (2008) 3598–3606.
[28] L. Robert, Hyaluronan, a truly "youthful" polysaccharide. Its medical applications, Pathol. Biol. (Paris) 63 (2015) 32–34.
[29] K.T. Dicker, L.A. Gurski, S. Pradhan-Bhatt, R.L. Witt, M.C. Farach-Carson, X. Jia, Hyaluronan: a simple polysaccharide with diverse biological functions, Acta Biomater. 10 (2014) 1558–1570.
[30] E. Stickeler, I.B. Runnebaum, V.J. Mobus, D.G. Kieback, R. Kreienberg, Expression of CD44 standard and variant isoforms v5, v6 and v7 in human ovarian cancer cell lines, Anticancer Res. 17 (1997) 1871–1876.
[31] S. Arpicco, P. Milla, B. Stella, F. Dosio, Hyaluronic acid conjugates as vectors for the active targeting of drugs, genes and nanocomposites in cancer treatment, Molecules 19 (2014) 3193–3230.
[32] S. Indraccolo, V. Tisato, S. Agata, L. Moserle, S. Ferrari, M. Callegaro, L. Persano, M.D. Palma, M.C. Scaini, G. Esposito, A. Fassina, O. Nicoletto, M. Plebani, L. Chieco-Bianchi, A. Amadori, E. D'Andrea, M. Montagna, Establishment and characterization of xenografts and cancer cell cultures derived from BRCA1 −/− epithelial ovarian cancers, Eur. J. Cancer 42 (2006) 1475–1483.
[33] K.J. Livak, T.D. Schmittgen, Analysis of relative gene expression data using real-time quantitative PCR and the 2(−Delta Delta C(T)) method, Methods 25 (2001) 402–408.
[34] M. Keyaerts, J. Verschueren, T.J. Bos, L.O. Tchouate-Gainkam, C. Peleman, K. Breckpot, C. Vanhove, V. Caveliers, A. Bossuyt, T. Lahoutte, Dynamic bioluminescence imaging for quantitative tumour burden assessment using IV or IP administration of D: -luciferin: effect on intensity, time kinetics and repeatability of photon emission, Eur. J. Nucl. Med. Mol. Imaging 35 (2008) 999–1007.
[35] V.K. Sharma, D.S. Kalonia, Temperature- and pH-induced multiple partially unfolded states of recombinant human interferon-alpha2a: possible implications in protein stability, Pharm. Res. 20 (2003) 1721–1729.
[36] E.C. Borden, T.F. Hogan, J.G. Voelkel, Comparative antiproliferative activity in vitro of natural interferons alpha and beta for diploid and transformed human cells, Cancer Res. 42 (1982) 4948–4953.
[37] S.D. Der, A. Zhou, B.R. Williams, R.H. Silverman, Identification of genes differentially regulated by interferon alpha, beta, or gamma using oligonucleotide arrays, Proc. Natl. Acad. Sci. U. S. A. 95 (1998) 15623–15628.
[38] J.A. Yang, K. Park, H. Jung, H. Kim, S.W. Hong, S.K. Yoon, S.K. Hahn, Target specific hyaluronic acid-interferon alpha conjugate for the treatment of hepatitis C virus infection, Biomaterials 32 (2011) 8722–8729.
[39] V.N.D. Le, M.S. Patterson, T.J. Farrell, J.E. Hayward, Q. Fang, Experimental recovery of intrinsic fluorescence and fluorophore concentration in the presence of hemoglobin: spectral effect of scattering and absorption on fluorescence, J. Biomed. Opt. 20 (2015) 127003.
[40] A. Rehemtulla, L.D. Stegman, S.J. Cardozo, S. Gupta, D.E. Hall, C.H. Contag, B.D. Ross, Rapid and quantitative assessment of cancer treatment response using in vivo bioluminescence imaging, Neoplasia 2 (2000) 491–495.
[41] P.F. Bassi, A. Volpe, D. D'Agostino, G. Palermo, D. Renier, S. Franchini, A. Rosato, M. Racioppi, Paclitaxel-hyaluronic acid for intravesical therapy of bacillus Calmette-Guerin refractory carcinoma in situ of the bladder: results of a phase I study, J. Urol. 185 (2011) 445–449.
[42] A. Serafino, M. Zonfrillo, F. Andreola, R. Psaila, L. Mercuri, N. Moroni, D. Renier, M. Campisi, C. Secchieri, P. Pierimarchi, CD44-targeting for antitumor drug delivery: a new SN-38-hyaluronan bioconjugate for locoregional treatment of peritoneal carcinomatosis, Curr. Cancer Drug Targets 11 (2011) 572–585.
[43] I.M. Montagner, A. Merlo, D. Carpanese, G. Zuccolotto, D. Renier, M. Campisi, G. Pasut, P. Zanovello, A. Rosato, Drug conjugation to hyaluronan widens therapeutic indications for ovarian cancer, Oncoscience 2 (2015) 373–381.
[44] S. Pucciarelli, L. Codello, A. Rosato, P. Del Bianco, G. Vecchiato, M. Lise, Effect of antiadhesive agents on peritoneal carcinomatosis in an experimental model, Br. J. Surg. 90 (2003) 66–71.
[45] A. Lewis, Y. Tang, S. Brocchini, J.W. Choi, A. Godwin, Poly(2-methacryloyloxyethyl phosphorylcholine) for protein conjugation, Bioconjug. Chem. 19 (2008) 2144–2155.
[46] E.J. Oh, K. Park, K.S. Kim, J. Kim, J.A. Yang, J.H. Kong, M.Y. Lee, A.S. Hoffman, S.K. Hahn, Target specific and long-acting delivery of protein, peptide, and nucleotide therapeutics using hyaluronic acid derivatives, J. Control. Release 141 (2010) 2–12.
[47] N. Forsberg, S. Gustafson, Characterization and purification of the hyaluronan-receptor on liver endothelial cells, Biochim. Biophys. Acta 1078 (1991) 12–18.